

RESEARCH

Open Access



Revealing heterogeneity in mild cognitive impairment based on individualized structural covariance network

Xiaotong Wei¹, Ronglong Xiong¹, Ping Xu¹, Tingting Zhang¹, Junjun Zhang¹, Zhenlan Jin¹ and Ling Li^{1*}

Abstract

Background Mild cognitive impairment (MCI) is a heterogeneous disorder with significant individual variabilities in clinical and biological features. Abnormal inter-regional structural covariance suggests disruption of the brain structural network in MCI. Most studies have examined group-level structural covariance alterations while ignoring individual-level differences. Hence, we aimed to investigate the heterogeneity of MCI using individual differential structural covariance network (IDSCN) analysis.

Methods T1-weighted images of 596 MCI patients and 309 cognitively normal (CN) were collected from the ADNI database as discovery dataset, and 122 MCI and 117 CN from the OASIS-3 dataset as validation cohort. We constructed each patient's IDSCN using regional gray matter volume and applied K-means clustering analysis to identify MCI subtypes based on significantly altered covariance edges. Then, clinical features, brain structure, and gene expression profiles were evaluated for each subtype.

Results In the ADNI dataset, MCI patients exhibited significant alterations in structural covariance edges, mainly involving the hippocampus, parahippocampal gyrus, and amygdala. Two robust MCI subtypes were identified. Subtype 1 showed faster disease progression relative to subtype 2, which was validated in the independent OASIS-3 dataset. Significant differences between two subtypes were found in clinical cognition and biomarkers, cerebral atrophy patterns, and enriched genes for metal ion transport and neuron projection development. Finally, correlation analysis and functional annotation further revealed that the affected edges were related to cognitive performance and implicated in memory and emotion terms.

Conclusions In summary, these findings offer new perspectives into understanding the heterogeneity of MCI and facilitate strategies for future precision medicine.

Keywords Mild cognitive impairment, Heterogeneity, Individual differential structural covariance network, Gray matter volume, Subtypes, Gene expression

*Correspondence:

Ling Li
liling@uestc.edu.cn

¹MOE Key Lab for Neuroinformaton, School of Life Science and Technology, The Clinical Hospital of Chengdu Brain Science Institute, University of Electronic Science and Technology of China, Chengdu 610054, China



© The Author(s) 2025. **Open Access** This article is licensed under a Creative Commons Attribution-NonCommercial-NoDerivatives 4.0 International License, which permits any non-commercial use, sharing, distribution and reproduction in any medium or format, as long as you give appropriate credit to the original author(s) and the source, provide a link to the Creative Commons licence, and indicate if you modified the licensed material. You do not have permission under this licence to share adapted material derived from this article or parts of it. The images or other third party material in this article are included in the article's Creative Commons licence, unless indicated otherwise in a credit line to the material. If material is not included in the article's Creative Commons licence and your intended use is not permitted by statutory regulation or exceeds the permitted use, you will need to obtain permission directly from the copyright holder. To view a copy of this licence, visit <http://creativecommons.org/licenses/by-nc-nd/4.0/>.

Introduction

Mild cognitive impairment (MCI) is usually considered a transitional phase between normal aging and Alzheimer's Disease (AD) and exhibits significant phenotypic heterogeneity in clinical symptoms, neuroimaging performance, and clinical progression [1–4]. MCI patients are at a high risk of progressing AD, with an annual conversion rate of approximately 10–15% [5]. While some individuals with MCI remain stable or even return to normal cognitive status after several years of follow-up [6, 7]. High level of heterogeneity in patient population can increase the difficulty of clinical trials and precision medicine. Therefore, exploring the heterogeneity of MCI is essential to reveal different phenotypes and further promote personalized prevention and treatment [8, 9].

To address this heterogeneity, clinicians often classify MCI patients according to clinical presentation and cognitive domain impairments, which can be divided into amnesic or non-amnesic types, and single-domain or multi-domain [10]. Although cognition-based subtyping has shown advantages in characterizing different dimensions of cognitive performance in MCI [11, 12], it still has several limitations, such as the neglect of neuroanatomical pathophysiological factors, indistinct boundaries, and restricted validity [13]. In recent years, more studies have adopted objective quantification such as magnetic resonance imaging (MRI) to resolve the heterogeneity of MCI [14–17], as MRI technology can accurately detect the underlying pathological changes in the early stages of disease compared to clinical performance [18, 19]. For example, the brain atrophy patterns of MCI patients show sufficient heterogeneity, and individuals can be divided into biologically and clinically meaningful subtypes [20]. In addition, data-driven methods have recently been applied to subtype studies of MCI based on structural MRI-derived biological features, such as gray matter morphometric characteristics [21, 22]. In contrast to manual subtyping by clinicians using conventional diagnostic guidelines, data-driven techniques focus on detecting the intrinsic stratified structure within unlabeled data. Despite their complexity, these methods are more objective and capable of reproducibly identifying potential disease subtypes from high-dimensional neuroimaging features that are difficult to distinguish visually, thereby providing more comprehensive and accurate support for clinical diagnosis and treatment [23, 24].

Preceding MRI studies have indicated brain morphological alterations in MCI patients, particularly in the hippocampus and medial temporal lobe [25, 26]. Nevertheless, these studies focused primarily on alterations in local anatomical regions and failed to consider the potential connections among distributed brain regions [27]. The structural covariance network (SCN) has been used to investigate the similarities and alterations of

morphological features in different brain regions, thereby elucidating the patterns of structural interconnectivity among these regions [28, 29]. Severe SCN disruption has been found in both MCI and AD patients [30]. Many conventional case-control studies have primarily detected differences at the group level; little is known about inter-individual heterogeneity [31, 32]. To explore individualized structural covariance differences, Liu et al. proposed a novel method to construct individual differential structural covariance network (IDSCN) [33]. IDSCN is constructed at the individual level and takes into account information from the control group, which can quantify the degree of deviation in structural covariance of each patient relative to the control group, providing a new perspective for parsing morphological heterogeneity [33]. Thus, employing a data-driven clustering analysis based on the IDSCN, we hypothesized that MCI patients could be classified into distinct subtypes with various patterns of cognitive performance, longitudinal progression, and brain morphology.

In this study, we aimed to investigate the heterogeneity of MCI based on the IDSCN analysis method. First, we constructed each patient's IDSCN using regional gray matter volume (GMV). Second, significantly altered structural covariance edges were regarded as features to classify MCI individuals into different subtypes. Third, we compared differences in clinical performance, brain structure, and gene expression profiles between subtypes. Finally, we evaluated the association of significantly affected IDSCN edges with clinical cognition.

Methods

Participants

In this study, the discovery data were obtained from the Alzheimer's Disease Neuroimaging Initiative (ADNI) 1/GO/2/3 datasets (<http://adni.loni.usc.edu>) and independent validation data from the Open Access Series of Imaging Studies-3 (OASIS-3) cohort (<https://www.oasis-brains.org/>) [34]. All participants or their authorized representatives offered written informed consent. For the ADNI dataset, we first enrolled cognitively normal (CN) and MCI subjects based on the reported diagnosis and published criteria [35]. Then, we determined disease stage during the follow-up based on the Clinical Dementia Rating Scale Sum of Boxes (CDRSB) scores [36–38]: CDRSB scores = 0 for normal cognitive stage, CDRSB scores from 0.5 to 4 for MCI stage, and CDRSB scores ≥ 4.5 for dementia stage. For selected CN subjects, their cognition remained normal at the first visit and follow-up (CDRSB = 0). The CDRSB scores of MCI patients ranged from 0.5 to 4 at inclusion. Based on changes in disease status during follow-up, the selected MCI patients were further divided into three subgroups: converters (MCI_C), who eventually progressed to AD

(CDRSB ≥ 4.5) during follow-up; stable MCI (MCI_S), who did not progress to dementia or revert to CN during follow-up; reverters (MCI_R), who finally reverted to normal during follow-up. For the OASIS-3 dataset, we enrolled CN patients with normal cognition at all follow-ups (CDR=0) and MCI patients with a CDR of 0.5 at inclusion. After a series of quality control steps (see Supplementary Fig. 1), the 309 CN and 596 MCI (including 276 MCI_C, 279 MCI_S, and 41 MCI_R) in ADNI and 117 CN and 122 MCI in OASIS-3 were finally recruited in the formal analyses. Several clinical measures were included in this study: the Alzheimer's Disease Assessment Scale-cognitive subscale (ADAS11 and ADAS13) [39], the CDRSB [36], the Mini-Mental State Examination (MMSE) [40], the Rey Auditory Verbal Learning Test (RAVLT, including immediate recall and learning) [41], cognitive domain composite scores (including memory, executive, language, and visuospatial ability), fludeoxyglucose (FDG), cerebrospinal fluid (CSF) amyloid- β (A β), CSF Tau, and CSF P-tau levels.

MRI data acquisition and preprocessing

The detailed structural MRI (sMRI) acquisition information was available on the ADNI and OASIS websites: <https://adni.loni.usc.edu/data-samples/adni-data/neuroimaging/mri/> and <https://www.oasis-brains.org/>. All T1-weighted (T1W) sMRI data were processed using a standard voxel-based morphometry (VBM) pipeline described in Supplementary Method S1: anterior commissure alignment, segmentation, normalization, modulation, and smooth. The Automated Anatomical Labeling (AAL) atlas was used to parcel the cerebrum into 90 cortical and subcortical regions [42] (Supplementary Table 3), and the average GMV of each cerebral region of each subject scan was extracted. Finally, the intracranial volume (ICV) was also calculated for the following analysis.

Constructing the IDSCN

We employed a recently proposed approach to build the IDSCN for each MCI patient according to regional GMV derived from the T1W image [33]. Prior to this, ComBat harmonization was applied to eliminate the site bias of gray matter maps with age and gender as covariates [43] (Supplementary Method S2). The main steps for constructing the IDSCN are summarized as follows (see Fig. 1): (1) with age, gender, education, and ICV as covariates, the partial Pearson correlation (PCC) between regional GMV for each pair of brain regions was calculated to construct a reference SCN in the CN group (PCC_n , n is the number of CN). (2) We added a patient k with MCI to the CN group to build a perturbed SCN in the same way as above (PCC_{n+1}). (3) The difference between the perturbed SCN and the reference SCN was calculated (i.e., $\Delta PCC_n = PCC_{n+1} - PCC_n$). (4) The

Z-scores of ΔPCC_n were calculated according to the following formula:

$$Z = \frac{\Delta PCC_n}{\frac{1 - PCC_n^2}{n-1}} \quad (1)$$

Edges with positive Z-scores in the patient's IDSCN of edges indicated higher structural covariance strength than the reference CN group, and vice versa. The P-values of edges in the IDSCN were transformed from the Z-scores. Finally, edges that were significantly different from the reference network for each patient were determined by Bonferroni correction ($P < 0.05$, $90 \times 89/2 = 4005$ edges).

Subtyping MCI using the IDSCN

As illustrated in Fig. 1, we divided MCI patients into subtypes by performing K-means cluster analysis. First, the number of patients with significant alterations was calculated for each edge in the IDSCN ($P < 0.05/4005$, Bonferroni correction). Then, all edges were ranked based on the number of patients with significant changes (from large to small), and we selected the top 40 edges as features for cluster analysis, as these edges were altered in at least 6% of patients [33, 44, 45]. An automatic grid search strategy was employed to optimize the best hyperparameters for K-means clustering model [46, 47]. To consider both clustering distinguishability and repeatability, the multiplication of the Calinski-Harabasz Index (CHI) and Adjusted Rand Index (ARI) is perceived as an index to determine the best clustering hyperparameters and number of clusters (highest CHI \times ARI) (Supplementary Method S3) [47]. We defined cluster numbers from 2 to 10 and replication number as 100 times. Finally, the best result for K-means is 2 clusters (highest CHI \times ARI = 226.496, Supplementary Fig. 4B). To determine whether Z-scores on these top 40 edges of the IDSCN differed significantly between two subtypes, a two-sample t-test was performed with age, gender, education, and ICV as covariates ($P < 0.05/40$, Bonferroni correction).

Statistical analysis

Demographic data

A two-sample t-test was used to compare differences in continuous variables between the CN and MCI groups ($P < 0.05$). The chi-square test was used to compare differences in categorical variables ($P < 0.05$). In addition, we also compared differences in demographic and clinical characteristics among three MCI subgroups using one-way analysis of variance (ANOVA, $P < 0.05$). The demographic data were analyzed using SPSS version 26.0.

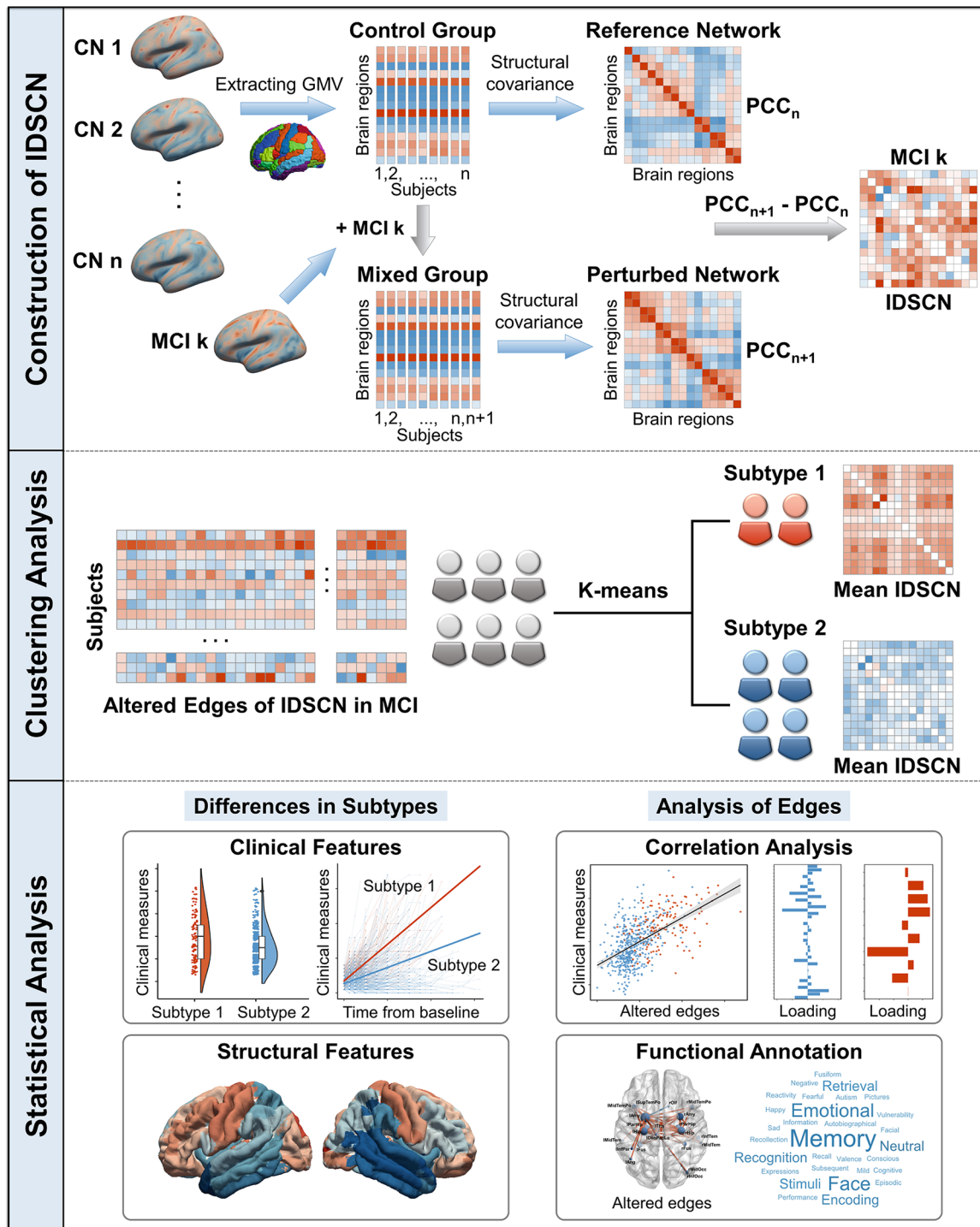


Fig. 1 A schematic summary of the study design. (1) The top part represents the workflow of constructing IDSCN. First, a reference structural covariance network was constructed across all controls, where the edges represented partial Pearson correlations between the GMV for each pair of regions (PCC_n) with age, gender, education, and ICV as covariates. Then, the added MCI k and all controls formed a new group to construct a perturbed network (PCC_{n+1}). Finally, the IDSCN of MCI k was the Z-score of the difference between the perturbed network and the reference network. (2) The middle part represents the clustering analysis of MCI patients using K-means. (3) The bottom part represents statistical analysis, including comparisons of characteristics between subtypes and analysis of covariance edges. Abbreviations: CN = cognitively normal; GMV = gray matter volume; ICV = intracranial volume; IDSCN = individual differential structural covariance network; MCI = mild cognitive impairment; PCC = partial Pearson correlation

Differences in clinical measures between subtypes

First, we compared cognitive scores, FDG, CSF A β , CSF Tau, and CSF P-tau measures across MCI subtypes and CN group using one-way ANOVA ($P < 0.05/14$, Bonferroni correction). The subjects were divided into four subgroups in MCI subtypes and CN group: A β -&Tau-, A β -&Tau+, A β +&Tau-, and A β +&Tau+. According to previous studies [20, 48], A β + was defined as A β < 976.6 pg/ml, and Tau+ was defined as P-tau > 21.8 pg/ml. The chi-square test was applied to examine the statistical significance of the ratio of four CSF biomarker levels. To further assess the potential impact of A β status, we performed a two-way ANOVA to examine the interaction between group (subtype 1, subtype 2, CN) and A β status (A β + vs. A β -) on clinical cognition and brain structure ($P < 0.05$, Bonferroni correction) (Supplementary Method S4).

For each MCI subtype, a Kaplan-Meier survival curve was then computed based on follow-up visits to assess the probability of conversion to AD. In this survival analysis, end event was defined as the time when MCI patients were first diagnosed with AD during follow-up. A log-rank test was adopted to compare survival curves between MCI subtypes. In addition, to further investigate the patterns of cognitive progression in MCI subtypes, a linear mixed-effects (LME) model was used to delineate cognitive decline trajectories as a function of follow-up time. The LME model, incorporating both fixed and random effects, is suitable for data with irregular follow-up intervals and missing time points [49]. Subject-specific random intercepts and slope terms as well as site-specific random intercepts were considered as random effects. Besides, age, sex, and education were regarded as fixed nuisance covariates. The linear time main effects and interaction effects were estimated separately using T-tests to obtain T-statistics and P-values ($P < 0.05/10$, Bonferroni correction). The LME model was performed using MATLAB 2020 (<https://www.mathworks.com/>). The model is described in Eq. (2):

$$\begin{aligned} \text{Cognitions} = & \\ & \beta_1 \text{Sub1} + \beta_2 (\text{Sub1} * \text{Time}) \\ & + \beta_3 \text{Sub2} + \beta_4 (\text{Sub2} * \text{Time}) \quad (2) \\ & + \beta_5 \text{Age} + \beta_6 \text{Sex} + \beta_7 \text{Edu} \\ & + (1 + \text{Time} | \text{Subject}) + (1 | \text{Site}) \end{aligned}$$

Differences in cerebral atrophy pattern between subtypes and relationship with gene expression

To compare the GMV of 90 cerebral regions among two MCI subtypes and CN, a one-way ANOVA was performed with age, gender, education, and ICV as covariates ($P < 0.05/90$, Bonferroni correction). Then, to further identify cerebral subregions whose atrophic trajectories

differed between MCI subtypes, we modeled the atrophic trajectories during follow-up time for MCI subtypes and their interactions on the atrophic process. This model was similar to Eq. (2), except that the dependent variable was GMV instead of Cognitions and ICV was added as a covariate ($P < 0.05/90$, Bonferroni correction, Eq. (3)). As apolipoprotein E (APOE) $\epsilon 4$ is the most influential genetic risk factor for AD [50], we used two-way ANOVA and the LME model to evaluate the influence of APOE genotype on the GMV of 90 cerebral regions and their longitudinal atrophic trajectories in MCI subtypes (Supplementary Method S5).

$$\begin{aligned} \text{GMV} = & \\ & \beta_1 \text{Sub1} + \beta_2 (\text{Sub1} * \text{Time}) \\ & + \beta_3 \text{Sub2} + \beta_4 (\text{Sub2} * \text{Time}) \quad (3) \\ & + \beta_5 \text{Age} + \beta_6 \text{Sex} + \beta_7 \text{Edu} + \beta_8 \text{ICV} \\ & + (1 + \text{Time} | \text{Subject}) + (1 | \text{Site}) \end{aligned}$$

Additionally, we investigated the relationship between the differential map of cerebral longitudinal atrophy patterns in MCI subtypes and regional gene expression. Gene expression data of six postmortem neurotypical adult brains with 3702 spatially distinct samples were obtained from the Allen Human Brain Atlas database (AHBA, <http://human.brain-map.org>) (Supplementary Table 4). We used the *abagen* toolkit (<https://github.com/rmarkello/abagen>) to process gene expression data according to a newly proposed pipeline (Supplementary Method S6) [51]. A gene expression matrix (90 regions \times 15,633 genes) with transcriptional level values was obtained. Then, a partial least squares (PLS) regression was performed to estimate the correlation between differences in longitudinal atrophy of MCI subtypes (T-values for 90 regions) and gene expression of 15,633 genes [52]. The gene expression matrix (90 regions \times 15,633 genes) was used as predictor variables, and the T vector (90 regions \times 1) was treated as response variables. The first component of the PLS (PLS1) was the linear combination of weighted gene expression scores, which was most strongly correlated with the longitudinal cerebral atrophic differences map of MCI subtypes. We adopted a spatial autocorrelation-preserving permutation test to assess the significance of correlation and bootstrapping method to obtain gene weights [53–55] (Supplementary Method S7). Finally, gene enrichment analysis was performed on the Metascape website (<https://metascape.org/gp/index.html>), including Gene Ontology (GO) of biological process, molecular function, cellular component, and the Kyoto Encyclopedia of Genes and Genomes (KEGG) pathway [56]. All pathways were corrected by the false discovery rate (FDR) with significance at $P < 0.05$.

Correlation analysis and functional annotation of altered structural covariance edges

Next, we introduced canonical correlation analysis (CCA) to test the relationships between the top 40 significantly altered edges of the IDSCN and the ten clinical cognitive measures in MCI patients ($P < 0.05$). To restrict the influence of underlying confounders on CCA results, we regressed age, gender, education, and ICV out of imaging data, and regressed age, gender, and education out of cognitive data. Besides, functional annotation analysis was performed to explore the potential clinical implications of these significantly altered edges using the Brain Annotation Toolbox (BAT, https://istbi.fudan.edu.cn/lnen/software/BAT_V1.1.rar). The BAT toolbox can provide voxel-level functional descriptions from the Neurosynth database and determine the functions associated with the networks generated by a region-based approach [57]. The significance of these altered structural covariance edges associated with functional terms was determined by a permutation test (10,000 times, $P < 0.001$, FDR correction).

Reproducibility analysis

To further validate the reproducibility of clustering results, we adopted the following strategies: (1) adopting other brain atlases, such as AAL2 (94 cerebral regions) [58], AAL3 (140 cerebral regions) [59], Brainnetome atlas (BN246, 246 cerebral regions) [60]; (2) using distinct numbers of top edges in the IDSCN, including top 102 edges altered in at least 5% of patients and top 13 edges altered in at least 7% of patients; (3) without ComBat harmonization. The ARI value was used as an index to evaluate the robustness of subtyping results [61]; (4) validation on an independent OASIS-3 dataset using the same methods as described above.

Results

Demographics and clinical characteristics

For the ADNI dataset, the demographic and clinical characteristics of the CN and MCI groups are presented in Table 1. There were no significant differences between CN and MCI groups in age ($t = -0.23$, $P = 0.820$) and gender ($\chi^2 = 3.32$, $P = 0.068$). The MCI patients had significantly lower educational years ($t = 3.33$, $P = 0.001$), worse cognitive functions, lower FDG, lower CSF A β , higher CSF Tau and P-tau levels, and a higher ratio of *APOE* $\epsilon 4$

Table 1 Main demographic and clinical characteristics of participants

Characteristic	CN	MCI	Statistics	P values
Demographics				
Number of subjects	309	596	-	-
Age (years)	74.09 \pm 5.91	74.19 \pm 7.10	$t = -0.23$	0.820
Gender (males/females)	164/145	354/242	$\chi^2 = 3.32$	0.068
Education (years)	16.60 \pm 2.62	15.95 \pm 2.82	$t = 3.33$	0.001
Clinical domains				
MMSE	29.03 \pm 1.19	27.45 \pm 1.88	$t = 15.44$	<0.001
ADAS11	5.73 \pm 2.79	10.78 \pm 4.63	$t = -20.42$	<0.001
ADAS13	8.89 \pm 4.25	17.39 \pm 6.88	$t = -22.84$	<0.001
RAVLT immediate	44.99 \pm 9.85	32.86 \pm 10.07	$t = 17.31$	<0.001
RAVLT learning	6.05 \pm 2.24	3.90 \pm 2.58	$t = 13.03$	<0.001
CDRSB	0.00 \pm 0.00	1.58 \pm 0.89	$t = -43.33$	<0.001
Memory	0.98 \pm 0.47	0.14 \pm 0.53	$t = 24.47$	<0.001
Executive	0.76 \pm 0.49	0.28 \pm 0.55	$t = 13.52$	<0.001
Language	0.83 \pm 0.50	0.33 \pm 0.49	$t = 14.18$	<0.001
Visuospatial	0.59 \pm 0.44	0.37 \pm 0.55	$t = 6.59$	<0.001
Metabolic biomarkers				
Number of subjects	161	424	-	-
FDG	1.29 \pm 0.11	1.20 \pm 0.14	$t = 7.77$	<0.001
CSF biomarkers				
Number of subjects	154	391	-	-
A β	1256.09 \pm 442.30	889.99 \pm 415.14	$t = 8.85$	<0.001
Tau	222.67 \pm 82.15	302.68 \pm 130.20	$t = -8.57$	<0.001
P-tau	20.19 \pm 7.93	29.64 \pm 14.71	$t = -9.64$	<0.001
Genotype				
<i>APOE</i> $\epsilon 4$ (carriers/noncarriers) ^a	82/218	315/281	$\chi^2 = 52.66$	<0.001

Continuous variables are shown as "mean \pm standard deviation". P values in bold denote statistical significance. ^a*APOE* $\epsilon 4$ carriers indicate participants having one or two copies of $\epsilon 4$ alleles. *APOE* $\epsilon 4$ genotype, FDG, and CSF biomarkers were not available for all participants

carriers (all $P < 0.001$) than the CN group. Additionally, statistical differences in cognitive scores, FDG, CSF biomarkers, and the ratio of *APOE* $\epsilon 4$ carriers were found among the MCI_C, MCI_S, and MCI_R subgroups (all $P < 0.001$), except for visuospatial ability ($F = 2.61$, $P = 0.074$) (Supplementary Table 1). For the OASIS-3 dataset, the CN and MCI groups did not differ in age ($t = -0.03$, $P = 0.976$) and gender ($\chi^2 = 0.67$, $P = 0.413$), while MCI patients had significantly lower educational years ($t = 2.98$, $P = 0.003$) and MMSE scores ($t = 8.04$, $P < 0.001$) than the CN group (Supplementary Table 2).

Heterogeneity analysis of IDSCN

For each MCI patient, we constructed the IDSCN based on the AAL atlas consisting of 4005 edges. Each edge indicates how the covariance between two connected nodes of the patient deviates from the normative covariance observed in the control group. Among all edges, 3958 edges were significantly altered in at least one patient, and 3817 edges were significantly altered in at least two patients (Supplementary Fig. 2). In addition,

the average IDSCN across all MCI indicated that the regions constituting the hippocampal-parahippocampal-amygdala network were severely affected (Supplementary Fig. 3). To prioritize the significantly altered edges in most patients, the top 40 edges altered in at least 6% of MCI patients were selected as the classifying features, mainly including the connections associated with hippocampus, parahippocampal gyrus (PHG), amygdala, and temporal lobe (Fig. 2A-B). The degree of a node is defined as the number of edges directly connected to this node (or brain region) to assess the node's importance in information transmission and processing. We calculated the degrees of nodes involved in these 40 edges, the largest of which was the left amygdala, followed by the bilateral hippocampus (Fig. 2C).

Two distinct MCI subtypes identified by IDSCN

We utilized the Z-scores of the top 40 edges as features for conducting K-means cluster analysis. The best hyperparameters for K-means included the distance metric "city block" and the method for selecting

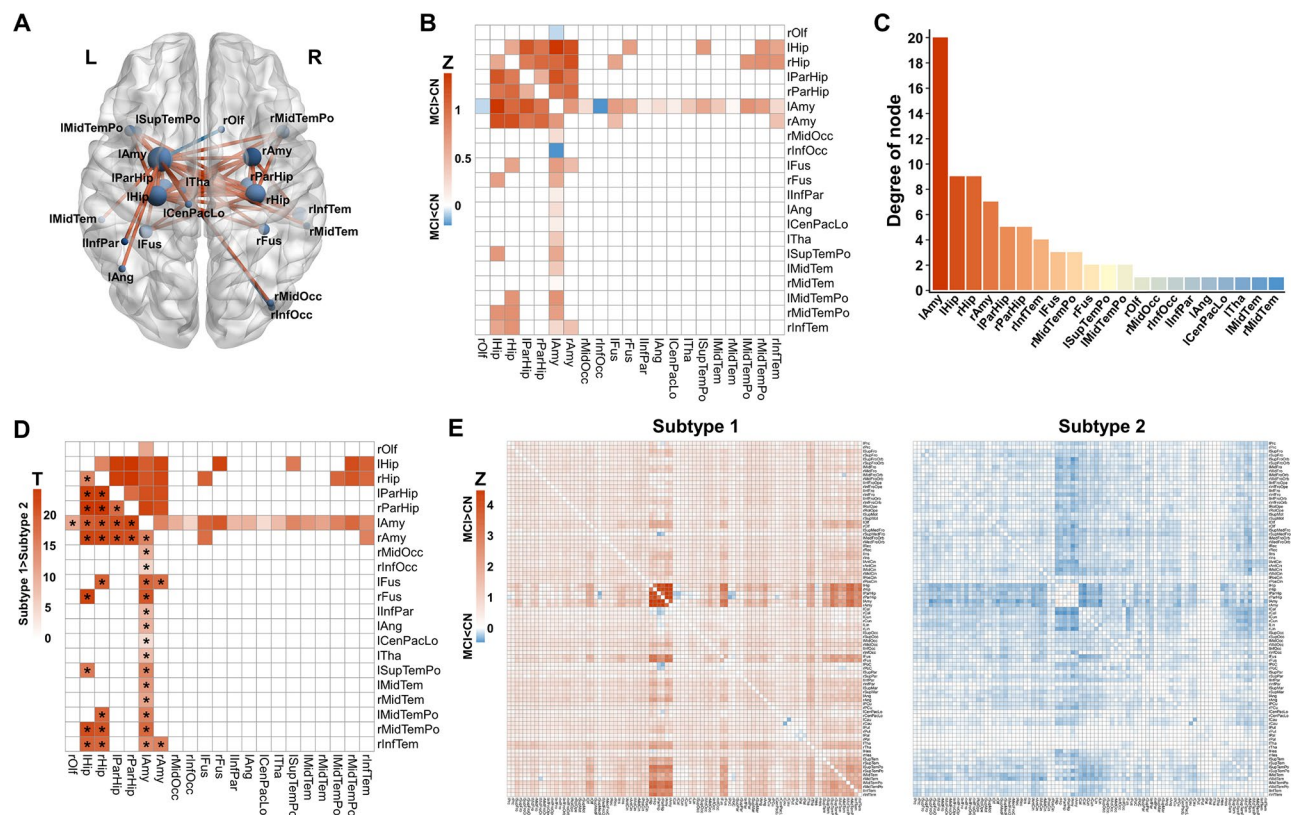


Fig. 2 Two MCI subtypes based on significantly altered covariance edges. **(A)** The brain map of the top 40 covariance edges significantly changed in at least 6% of patients. Red edges indicate Z-score > 0 and blue edges indicate Z-score < 0. The size of nodes is proportional to their degree. **(B)** The Z-score of the top 40 significantly altered covariance edges. **(C)** Degree of nodes involved in significantly altered covariance edges. **(D)** Group comparison results of the top 40 significantly altered covariance edges between two MCI subtypes using two-sample t-tests with age, gender, education, and ICV as covariates (subtype 1 vs. subtype 2). Asterisk (*) indicates structural covariance of significant differences between two subtypes ($P < 0.05/40$, Bonferroni correction). **(E)** The mean patterns of IDSCN for two MCI subtypes. The full names of the brain regions are shown in Supplementary Table 3. Abbreviations: CN = cognitively normal; ICV = intracranial volume; IDSCN = individual differential structural covariance network; MCI = mild cognitive impairment

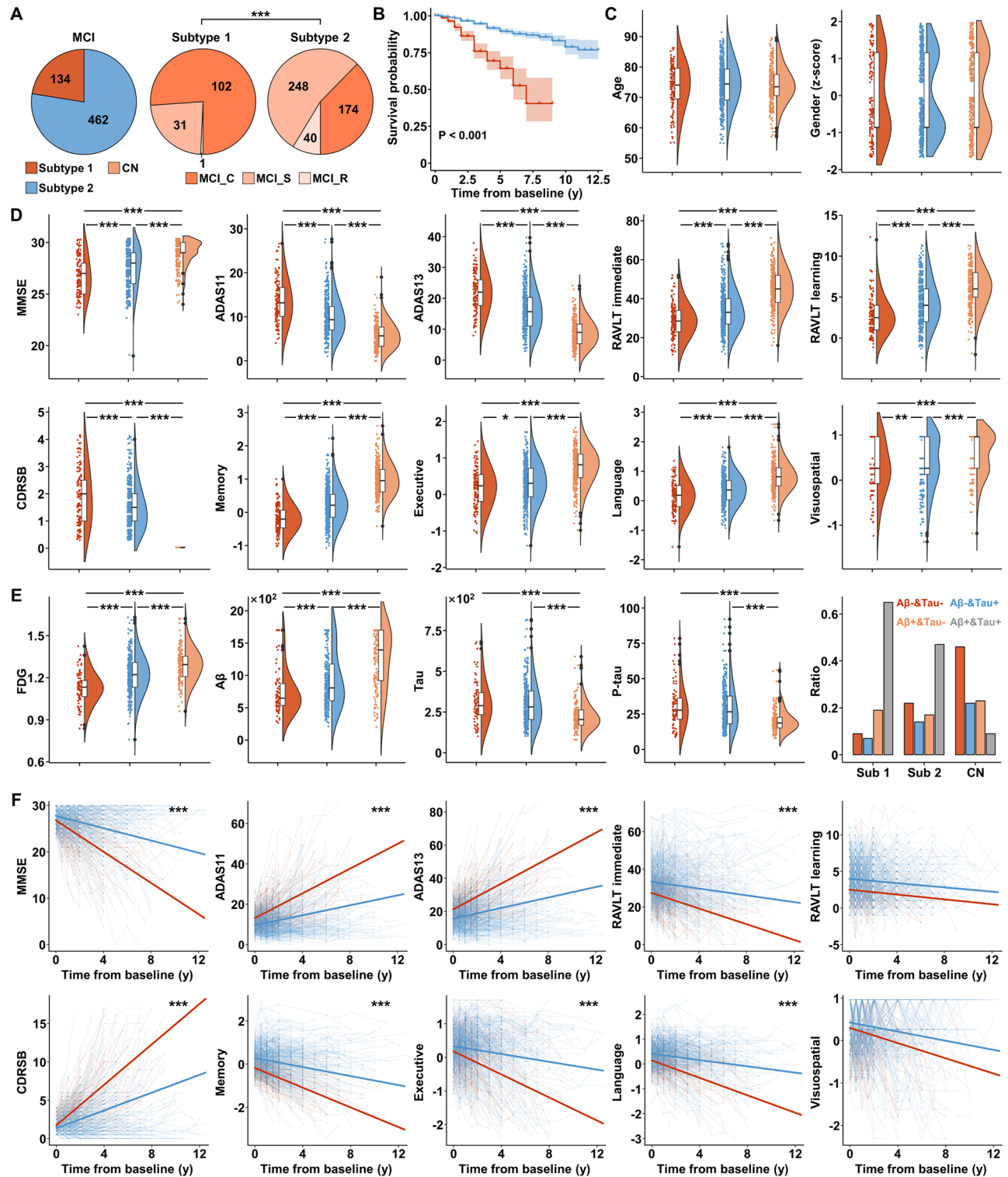


Fig. 3 (See legend on next page.)

initial cluster centroid positions “cluster”. The CHI × ARI index was maximum when the cluster was two (CHI × ARI=226.496, Supplementary Fig. 4B). The 596 MCI patients were clustered into two subtypes (subtype

1, $n=134$; subtype 2, $n=462$). Two-sample t-tests illustrated that subtype 1 had significantly higher Z-scores than subtype 2 in these 40 structural covariance edges ($P < 0.05/40$, Bonferroni correction, Fig. 2D). Moreover,

(See figure on previous page.)

Fig. 3 Comparisons of clinical characteristics between two MCI subtypes. **(A)** The pie chart on the left shows the number of subjects in subtype 1 and subtype 2. The two pie charts on the right show the number of clinical subgroups in subtype 1 and subtype 2, respectively. **(B)** Kaplan-Meier curves depict the probability of non-conversion to AD in subtype 1 (red) and subtype 2 (blue). Comparisons of demographics **(C)**, cognitive characteristics **(D)**, FDG values, and CSF biomarker levels **(E)** among the subtype 1, subtype 2, and CN. **(F)** Longitudinal changes in cognitive characteristics. Solid red (subtype 1) and blue (subtype 2) lines represent the fitted cognitive change as a function of follow-up time. * $P < 0.05$, ** $P < 0.01$, *** $P < 0.001$. Abbreviations: ADAS11 = Alzheimer's Disease Assessment Scale Cognitive-11; ADAS13 = Alzheimer's Disease Assessment Scale Cognitive-13; A β = amyloid- β ; CDRSB = Clinical Dementia Rating Scale Sum of Boxes; CN = cognitively normal; CSF = cerebrospinal fluid; FDG = fludeoxyglucose; MCI_C/MCI_S/MCI_R = mild cognitive impairment converters/stable/reverters; MMSE = Mini-Mental State Examination; P-tau = phosphorylated tau; RAVLT = Rey Auditory Verbal Learning Test; Sub = subtype; y = year

these two subtypes had distinct patterns of IDSCN profile (Fig. 2E and Supplementary Fig. 5).

Differences in demographics and clinical measures between MCI subtypes

The ratio of three MCI subgroups was significantly different between the two subtypes ($P < 0.001$, Fig. 3A). Survival analysis revealed that subtype 1 showed faster progression to AD relative to subtype 2 (log-rank test: $\chi^2 = 162.21$, $P < 0.001$, Fig. 3B). One-way ANOVA and chi-square test indicated statistical differences in education, cognitive scores, FDG, CSF biomarkers, and the proportion of *APOE* $\epsilon 4$ carriers (all $P < 0.001$) among two MCI subtypes and CN group, but there were no significant differences in age ($F = 0.91$, $P = 0.405$) and gender ($\chi^2 = 3.34$, $P = 0.189$) (Fig. 3C-E and Supplementary Table 5). Post hoc tests found that subtype 1 had worse cognitive functions, lower FDG, lower CSF A β levels, and a higher ratio of *APOE* $\epsilon 4$ carriers than subtype 2. However, there were no significant differences in CSF Tau and P-tau levels between two MCI subtypes ($P > 0.05$). In addition, the proportion of A β +&Tau+ in subtype 1 was higher than that in subtype 2, while the proportion of A β -&Tau- in subtype 1 was lower than that in subtype 2 ($P < 0.05$, Fig. 3E and Supplementary Table 6). Two-way ANOVA revealed the significant interaction between the three groups and two A β levels on ADAS13, CDRSB, memory scores, and GMV in the bilateral amygdala, bilateral superior temporal pole, and right middle temporal pole (Supplementary Results S1, Supplementary Tables 7–8 and Supplementary Fig. 6). After controlling for age, gender, and education, the LME models identified that subtype 1 had a faster rate of cognitive decline during follow-up than subtype 2 (all $P < 0.001$), except in the areas of RAVLT learning and visuospatial ability (Fig. 3F and Supplementary Table 9).

Cerebral atrophy of MCI subtypes and gene expression profiling

Among the 90 cerebral subregions, significant differences in GMV were observed between the two subtypes, with subtype 1 showing more pronounced atrophy than subtype 2, particularly in the bilateral hippocampus, PHG, and amygdala (Supplementary Fig. 7). LME identified 35 regions whose atrophic trajectories with follow-up time

in subtype 1 were faster than subtype 2, including the bilateral superior temporal pole, middle temporal pole, hippocampus, and so on ($P < 0.05/90$, Fig. 4B, Supplementary Fig. 8, and Supplementary Table 10). In addition, two-way ANOVA and LME model revealed the *APOE* $\epsilon 4$ has a significant effect on brain atrophy in both MCI subtypes, with *APOE* $\epsilon 4$ carriers exhibiting faster atrophic rates than noncarriers, particularly in the hippocampus, middle temporal gyrus, and inferior temporal gyrus (Supplementary Results S2, Supplementary Tables 11–12 and Supplementary Fig. 9–11).

The PLS regression can evaluate the associations between regional gene expression patterns and the T-map of the longitudinal atrophic difference between two subtypes (Fig. 4B). The PLS1 explained 53% of the variance in longitudinal cerebral atrophic differences of MCI subtypes, significantly more than expected by chance (spin test, $P_{\text{spin}} < 0.001$). The distribution of the PLS1 scores represented an anterior-posterior gradient of gene expression (Fig. 4C). Notably, the PLS1 gene expression map was positively associated with the T-map of longitudinal atrophic difference between the two subtypes ($R = 0.73$, $P_{\text{spin}} < 0.001$, Fig. 4A). As reported by prior research [55], we ranked the normalized weights of PLS1 based on each gene' Z-score. Overall, 4010 genes were recognized as making significant contributions to PLS1 ($P < 0.05$, FDR correction). Among them, 1795 genes exhibited positive normalized PLS1 weights (PLS1+, $Z > 4$), and 2215 genes exhibited negative normalized PLS1 weights (PLS1-, $Z < -4$). These positive correlations indicated that PLS1+ genes were overexpressed in regions with increased T values (e.g., *NCOA3*), while negative correlations indicated that PLS1- genes were overexpressed in regions with decreased T values (e.g., *IFT22* and *APOE*) (Fig. 4D-E). After correcting for enrichment analysis ($P < 0.05$, FDR correction), the PLS1+ gene set was mainly enriched for several significant GO pathways, such as "phosphorylation" and "metal ion transport" and KEGG pathways including "Pathways in cancer" (Fig. 4F). The PLS1- gene list was mainly enriched in GO pathways including "neuron projection development", "presynapse", and "axon" (Fig. 4G).

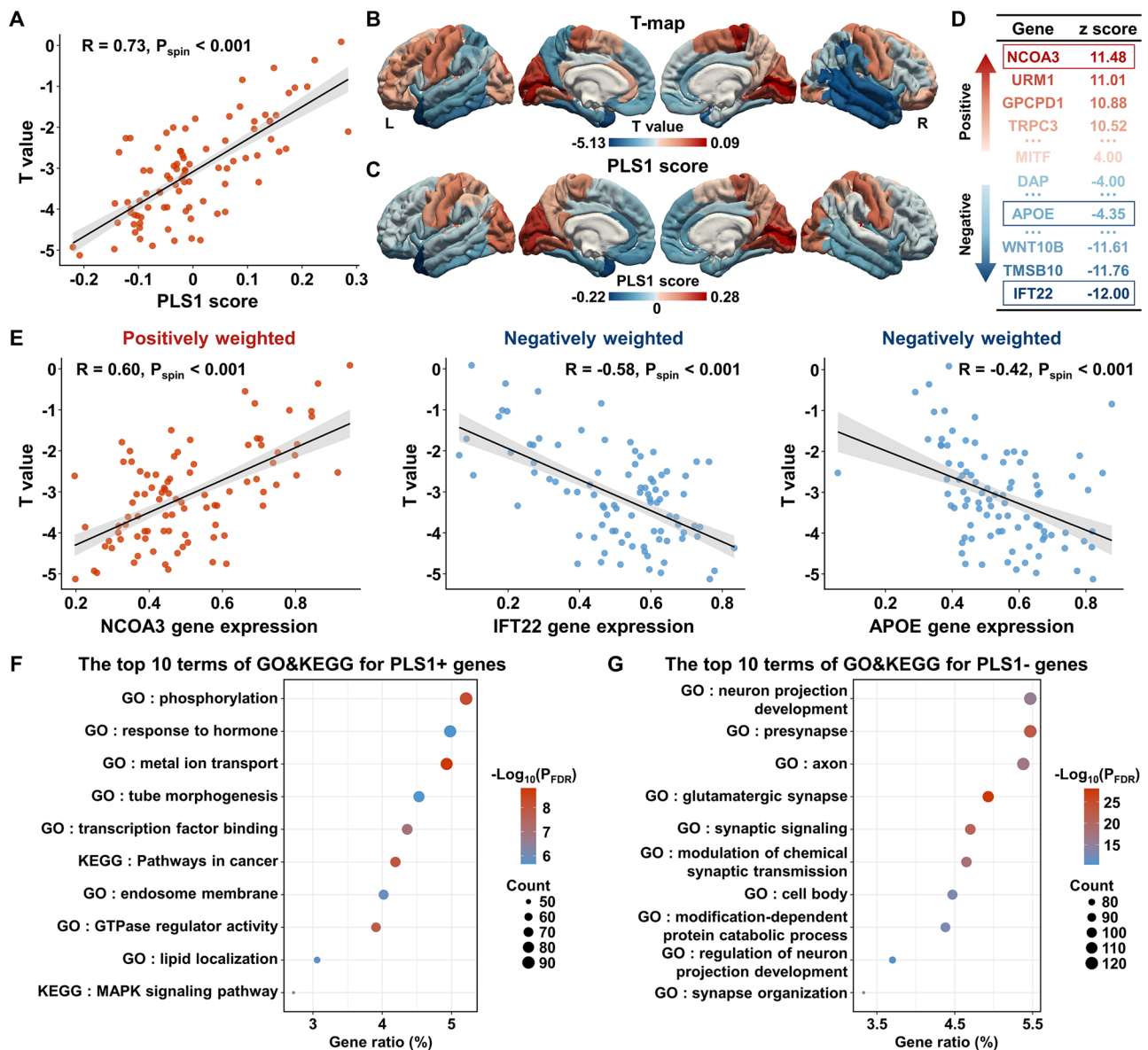


Fig. 4 Gene expression profiles related to the longitudinal cerebral atrophy differences of two MCI subtypes. **(A)** The correlation between regional PLS1 scores (weighted sum of 15,633 gene expression scores) and the T values of differences in longitudinal cerebral atrophy between two MCI subtypes. **(B)** The cortical maps of the subtype differences in cerebral atrophy as a function of follow-up time (subtype 1 vs. subtype 2). The color bar represents the T values without a threshold. **(C)** The cortical maps of regional PLS1 scores. The color bar represents the PLS1 scores without a threshold. **(D-E)** Genes positively weighted on PLS1 (e.g., *NCOA3*) are positively correlated with T values of subtype differences in longitudinal cerebral atrophy ($r = 0.60, P_{spin} < 0.001$), whereas genes negatively weighted on PLS1 (e.g., *IFT22* and *APOE*) are negatively correlated with T values of subtype differences in longitudinal cerebral atrophy ($r = -0.58$ and $r = -0.42, P_{spin} < 0.001$). Bubble plots show the top 10 GO and KEGG pathways for the PLS1+ genes **(F)** and PLS1- genes **(G)**, respectively. The bubble size represents the number of overlapped genes between the PLS1+ (or PLS1-) gene list and each GO term or KEGG pathway (y-axis). The x-axis represents the ratio of overlapped genes. The color bar represents the $-\log_{10}(P)$ values (FDR correction). Abbreviations: APOE=apolipoprotein E; FDR=false discovery rate; GO=Gene Ontology; KEGG=Kyoto Encyclopedia of Genes and Genomes; PLS=partial least squares

Correlation analysis and functional annotation of altered edges in IDSCN

According to CCA, we clarified the association between the top 40 edges that were significantly altered in MCI patients and clinical cognition. We found a significant positive correlation between the first canonical variable of the 40 covariance edges and that of 10 clinical

cognitive items ($R = 0.55, P < 0.001$, Fig. 5A). Furthermore, the covariance edges with left PHG-right amygdala were the principal contributors to the first canonical variable (loading value: $v = -0.83$, Fig. 5B). The memory item of cognitive domain composite primarily contributed to the first canonical variable of clinical cognition (loading value: $u = -0.56$, Fig. 5C). To further verify the underlying

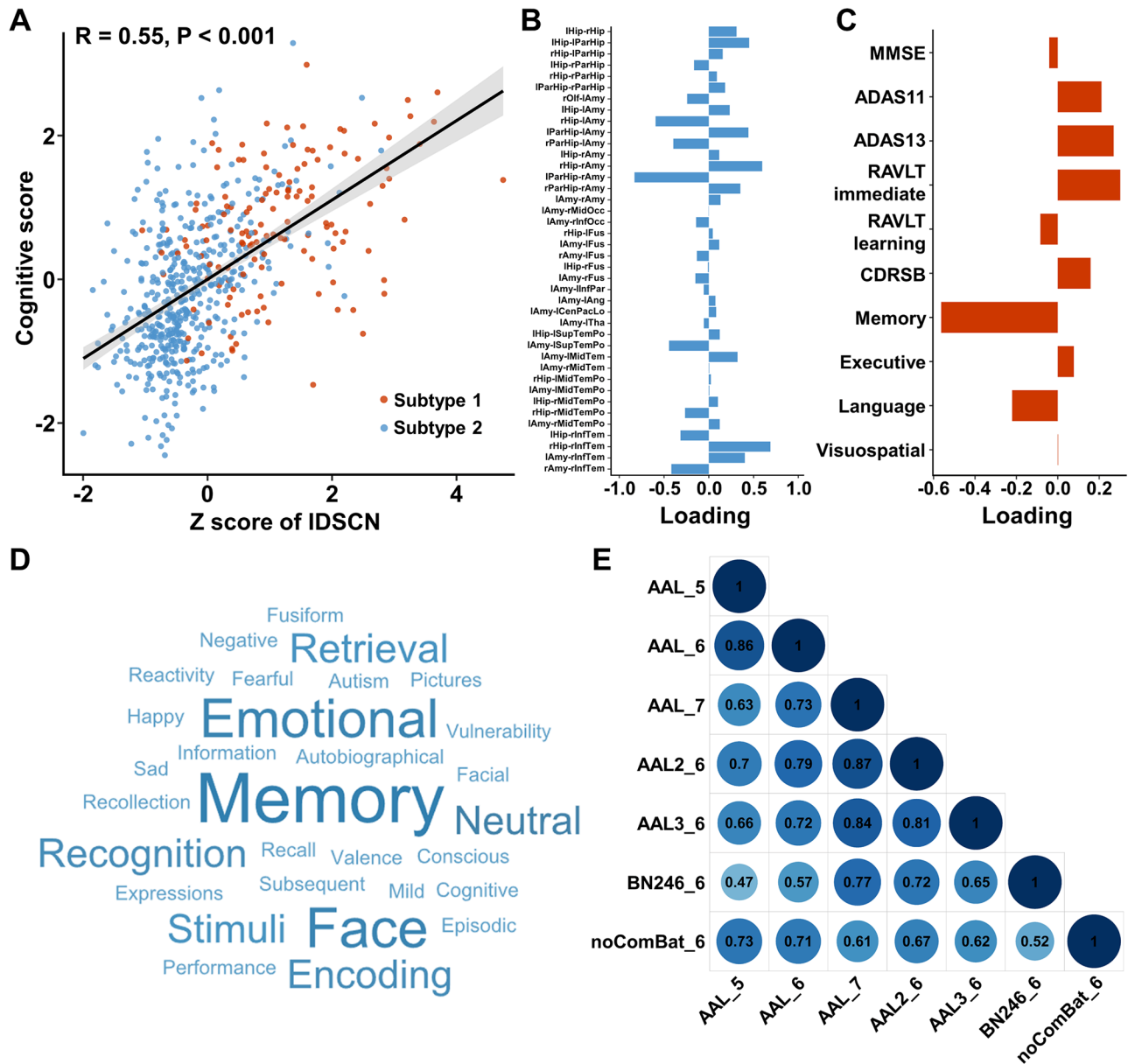


Fig. 5 Analysis of covariance edges. **(A)** The correlation between the first canonical variable of the top 40 covariance edges and that of 10 clinical cognitive items. **(B)** The canonical loadings of these top 40 covariance edges. **(C)** The canonical loadings of 10 clinical cognitive items. **(D)** The word cloud represents keywords for 30 significant functional terms obtained by functional annotation of these top 40 covariance edges ($P < 0.001$, FDR correction). The larger text indicates a higher frequency of keywords. These 30 functional terms are shown in Supplementary Table 13. **(E)** The ARI values between clustering results based on different brain atlases and numbers of top edges. For example, AAL_5 represented clustering results using the AAL atlas and the top edges that were changed in at least 5% of MCI patients. The full names of the brain regions are shown in Supplementary Table 3. Abbreviations: AAL = Automated Anatomical Labeling; ADAS11 = Alzheimer’s Disease Assessment Scale Cognitive-11; ADAS13 = Alzheimer’s Disease Assessment Scale Cognitive-13; ARI = Adjusted Rand Index; BN = Brainnetome atlas; CDRSB = Clinical Dementia Rating Scale Sum of Boxes; FDR = false discovery rate; MMSE = Mini-Mental State Examination; RAVLT = Rey Auditory Verbal Learning Test

functional implications of these 40 covariance edges, we performed a functional annotation analysis based on BAT. We found that 30 functional terms were significantly related to various functions such as memory and emotion ($P < 0.001$, FDR correction) (Fig. 5D and Supplementary Table 13).

Results of reproducibility analysis

Subtyping results showed robust consistency for various subtyping strategies. MCI patients were optimally classified into two subtypes with different brain atlases (AAL2, AAL3, BN246), number of top edges (top 102 or 13 edges significantly altered in at least 5% or 7% of patients), and without ComBat harmonization (Supplementary Fig. 4

and Supplementary Fig. 12–14). Besides, the ARI values were calculated to examine the consistency of subtyping results (Fig. 5E). The ARI between the main reported subtyping results (AAL_6) and those of 5% of patients (AAL_5) was 0.86, reflecting a good consistency. Moreover, the ARI between subtyping results using AAL2 atlas (AAL2_6) and top edges altered in at least 7% of patients (AAL_7) was 0.87. In the OASIS-3 dataset, using the same top 40 edges as features, MCI patients also were divided into two subtypes (Supplementary Fig. 15). Similar to the discovery data, subtype 1 had lower MMSE scores and faster decline than subtype 2. Survival analysis indicated a significant difference in progression to AD between two subtypes (log-rank test: $\chi^2=25.62$, $P<0.001$), with subtype 1 exhibiting more accelerated progression over time than subtype 2 (Supplementary Fig. 16).

Discussion

In the present study, a principal aim was to explore the heterogeneity of MCI patients by constructing IDSCN. First, we identified IDSCN for each patient relying on regional GMV. Individual patients exhibited notable differences in their IDSCNs at the network level. Despite this whole-brain heterogeneity, altered covariance edges involving the hippocampus, PHG, amygdala, and temporal lobe were often observed in most patients. Then, a data-driven approach was applied to identify two distinct subtypes of MCI, and we also demonstrated the clinical and biological validity of the two subtypes. Specifically, subtype 1 showed faster disease progression relative to subtype 2. The two subtypes showed distinct patterns in cognitive impairment, biomarker characteristics, cerebral atrophy, and regional gene expression. These results may provide a new perspective for understanding the heterogeneity of MCI.

It is well established that the brain is a complex network where neural activity is processed and integrated among different regions [62]. Large-scale structural covariance networks can capture the coordinated volumes between pairwise brain regions to reflect their synchronized maturation or atrophy, mutually trophic reinforcement, and common experience-driven plasticity [29, 63]. Previous studies reported abnormal structural covariance networks in MCI patients, including the limbic and medial temporal networks [31, 32, 64]. These outcomes suggested structural covariance aberrance at the population level while ignoring inter-individual differences. Recently, a novel method by constructing IDSCN has been used to address the individual heterogeneity of neuropsychiatric disorders, such as schizophrenia [33], depression [65], autism spectrum disorder [44], and AD [45], providing a new viewpoint for adopting individualized analysis methods in further neuroimaging studies.

As the prodromal stage of AD, MCI represents a critical window for clinical intervention, and its heterogeneity is particularly pronounced. To some extent, our study reinforces the awareness of individual differences in morphological networks of MCI, which is conducive to determining precision medicine strategies and personalized treatment plans.

In this research, we analyzed individual-level differential structural covariance networks in MCI patients, with edges representing the degree of deviation of each patient's structural covariance pattern from that of the healthy control group. In line with previous studies, we found low similarity of IDSCNs between patients and a reduced overlap of significantly altered edges with each other, indicating higher structural heterogeneity in MCI [3, 20]. Despite the observed heterogeneity, structural covariance connections between the hippocampus, PHG, amygdala, and temporal lobe were significantly affected in most patients, which may be a potential neural substrate for memory loss and cognitive impairment. Many studies have reported that MCI patients suffer severe gray matter atrophy and white matter fiber disruption in these regions, and these disruption affects the integrity of the stable network structure, thereby contributing to cognitive decline [66–68]. In the CCA examining relations between affected covariance edges and cognitive data, two canonical variates pairs were significant. The connectivity pattern most strongly associated with cognitive dimensions included the negative loading of edges within the left PHG and right amygdala. Furthermore, functional annotation demonstrated that these edges of IDSCN were mainly associated with memory, emotion, etc. In light of these outcomes, we assumed that alterations in structural covariance within these core regions may underlie cognitive dysfunction in MCI, particularly affecting processes such as memory formation and emotional regulation.

Extensive evidence manifests that individuals with MCI may be classified into distinct subtypes, such as cognition-based classifications (e.g., amnesic and non-amnesic) [4, 10, 69], risk stratification (e.g., high and low risk) [70, 71], and atrophy pattern comparisons (e.g., CN and AD-like atrophy) [20, 21]. These studies provide valuable insights into the clinical and pathological diversity of MCI, but do not appear to capture the neurodegeneration patterns at the individual level [72]. Our approach utilized IDSCN constructed from T1W images to detect patient-specific structural variations and offered a detailed classification framework. MCI patients were subdivided into two robust subtypes with various patterns of covariance edges (higher degree of deviation in subtype 1 than in subtype 2), while these individual differences may be overlooked in group-level analyses. In terms of clinical presentation, subtype 1 had worse

cognitive function and a faster rate of cognitive decline than subtype 2. Pathological differences in FDG and CSF A β levels were also found between two subtypes, which may reflect underlying variations in brain metabolic activity and A β accumulation. The higher proportion of abnormal CSF A β (A β +) and P-tau (Tau+) in subtype 1 indicated a significant role of amyloid and tau pathology, potentially driving more severe neurodegeneration and a higher risk of progression to AD [73, 74].

Subtype 1 included mainly MCI_C patients, while subtype 2 included mainly MCI_S and MCI_R patients. However, similar to the results of several subtype studies [20, 21], the identified two neurobiological subtypes do not completely overlap with traditional clinical subgroups, which may be due to multiple factors influencing the progression of MCI. Thus, we can only speculate that subtype 1 had a higher risk of progression to AD than subtype 2, which was also supported by differences in AD conversion rates between subtypes. The robustness of MCI subtypes was demonstrated by the repeatability of clustering subtypes in various parcellation schemes, edge selection, and the independent dataset. Interestingly, Zheng et al. [45] identified two distinct AD subtypes based on IDSCN analysis, including slow and rapid progression types, which is similar to our findings. These results suggest that there may be similar pathological features and potential links between MCI and AD subtypes, which need to be further verified.

We further demonstrated whether the two subtypes differed in their underlying patterns of brain morphological alterations. The results showed subtype 1 exhibited more severe and faster gray matter atrophy than subtype 2 during disease progression, particularly in the superior temporal pole, middle temporal pole, and hippocampus. These findings are in agreement with previous neuroanatomical studies, where MCI patients with faster GMV reduction have a relatively poor prognosis and a higher risk of progressing to AD [66]. These two distinct subtypes exhibited different atrophic patterns with underlying neurobiological significance. It is well-known that AD is impacted by multiple genetic risk factors, including the *APOE* ϵ 4 gene [75]. Consistent with previous studies, *APOE* ϵ 4 carriers showed faster atrophic rates than non-carriers in both MCI subtypes, particularly in the hippocampus and temporal lobes, suggesting that the *APOE* gene may play an important regulatory role in the brain atrophy of MCI [76, 77].

Recently, genome-imaging association analysis has become an effective tactic for exploring the molecular foundations of brain structural organization [54, 55]. Using multivariate PLS regression, we discovered that the map of longitudinal cerebral atrophic differences between two MCI subtypes showed spatial correlation with the gene expression map, and further detected

significantly weighted genes in the PLS1 that may be involved in the pathogenesis of MCI. The PLS1+ genes were generally overexpressed in occipital and parietal cortical areas of increased T values. Conversely, the PLS1- genes were generally overexpressed in frontal and temporal cortical areas of decreased T values. Gene set enrichment analysis revealed that the observed pathways were primarily implicated in metal ion transport, neuron projection development, and presynapse. Abnormalities or dysregulations of these pathways are associated with AD. An imbalance of metal ions can lead to oxidative stress, which in turn causes the phosphorylation of tau protein in neurons, deposition of A β amyloid, and damage to neuronal cells, which is closely associated with the onset of AD [78]. Loss of synapses and neuronal impairment have been reported to be important pathological factors in AD [79]. Besides, the trans-synaptic neuron-to-neuron disconnection syndrome within the central nervous system is a key mechanism in the pathology of MCI, and neurodegeneration-driven cognitive decline is a final common pathway in the dementia process [80]. In this study, MCI subtypes exhibited similar gene pathways as those in AD. These results elucidated the role of gene expression in modulating the brain structure of MCI.

The potential clinical implications of these findings included: (1) The IDSCN could capture individual-specific structural changes, and IDSCN-derived subtypes could further deepen our understanding of the biological heterogeneity of MCI. Compared to the cognitive subtypes, brain structural subtypes were relatively stable and sensitive than clinical symptoms in the early stages of disease, and may more closely reflect biological heterogeneity [72]. (2) Brain structural subtypes may help individualized diagnosis by resolving the inter-individual heterogeneities. It has been reported that the subtyping frameworks incorporating neuroanatomical features could improve the diagnostic accuracy of MCI patients [17]. Despite the challenges of implementing this approach in clinical practice, future research will be devoted to developing computer-aided diagnostic tools to facilitate its clinical application and serve as a valuable complement to other classification frameworks, such as visual rating scales [81, 82]. (3) Brain structural subtypes may help predict disease progression. This study found two subtypes: one with relatively rapid progression and the other with relatively slow progression. At present, early clinical intervention can effectively delay disease progression (e.g., cognitive training therapy, pharmacotherapy) [83]. The distinct MCI subtypes may require different treatment approaches and intervention strategies, which should be validated in the future [84].

Our studies have some limitations. First, our study was based on the ADNI and OASIS-3 databases. Validating the applicability of this subtyping framework in

larger populations is a critical step for future work. Second, due to the limitation of data acquisition, the disease state was determined based on reported diagnosis and CDRSB scores. Future studies should incorporate A β and tau measurements to more accurately confirm the disease state. Third, because gray matter loss is frequently detected in the MCI stage, we constructed the IDSCN using only GMV. Future studies should integrate clinical symptoms, multimodal neuroimaging and pathology data to systematically uncover MCI heterogeneity, and explore the relationship between structural subtypes and other modal subtypes (e.g., cognitive, functional, PET-derived subtypes) for cross-study comparisons. Finally, MCI may progress to other non-AD types of dementia, more detailed subtype analyses in future larger cohorts are essential.

Conclusion

Based on IDSCN analysis, this study emphasizes the individual heterogeneity of brain structure in MCI patients. According to individual heterogeneity, two MCI subtypes with different clinical features, patterns of brain structure, and gene expression profiles were determined. Overall, these findings offer an important viewpoint into the morphological heterogeneity of MCI from the perspective of individual differences. This study also lays a solid foundation for the development of personalized therapies based on the IDSCN stratification and the advancement of precision medicine.

Supplementary Information

The online version contains supplementary material available at <https://doi.org/10.1186/s13195-025-01752-4>.

Supplementary Material 1

Acknowledgements

Data collection and sharing for this project were funded by the Alzheimer's Disease Neuroimaging Initiative (ADNI) (National Institutes of Health Grant No. U01 AG024904) and DOD ADNI (Department of Defense Award Number W81XWH-12-2-0012). ADNI is funded by the National Institute on Aging, the National Institute of Biomedical Imaging and Bioengineering, and through generous contributions from the following: AbbVie, Alzheimer's Association; Alzheimer's Drug Discovery Foundation; Araclon Biotech; BioClinica, Inc.; Biogen; Bristol-Myers Squibb Company; CereSpir, Inc.; Cogstate; Eisai Co., Inc.; Elan Pharmaceuticals, Inc.; Eli Lilly and Company; EuroImmun; F. Hoffmann-La Roche Ltd and its affiliated company Genentech, Inc.; Fujirebio; GE Healthcare; IXICO Ltd.; Janssen Alzheimer Immunotherapy Research & Development, LLC.; Johnson & Johnson Pharmaceutical Research & Development, LLC.; Lumosity; Lundbeck; Merck & Co., Inc.; Meso Scale Diagnostics, LLC.; NeuroRx Research; Neurotrack Technologies; Novartis Pharmaceuticals Corporation; Pfizer Inc.; Piramal Imaging; Servier; Takeda Pharmaceutical Company; and Transition Therapeutics. The Canadian Institutes of Health Research provides funds to support ADNI clinical sites in Canada. Private sector contributions are facilitated by the Foundation for the National Institutes of Health (<http://www.fnih.org>). The grantee organization is the Northern California Institute for Research and Education, and the study is coordinated by the Alzheimer's Therapeutic Research Institute at the University of Southern California. ADNI data are disseminated by the Laboratory for Neuro Imaging at the University

of Southern California. Validation data used in this study were provided by the OASIS-3 database (<https://www.oasis-brains.org/>). OASIS-3: longitudinal multimodal neuroimaging; principal investigators: T. Benzinger, D. Marcus, J. Morris; NIH P30 AG066444, P50 AG00561, P30 NS09857781, P01 AG026276, P01 AG003991, R01 AG043434, UL1 TR000448, R01 EB009352. The authors would like to acknowledge Liang Tan, Xiaotong Du, and Yu Zhang for their guidance in data analyses.

Author contributions

X.W. & L.L. contributed to the design of research; X.W. & R.X. contributed to data analysis; P.X., T.Z., J.Z., Z.J. & L.L. provided guidance and advice. X.W. & L.L. contributed to the writing of the manuscript.

Funding

This research was supported by grants from the National Natural Science Foundation of China (62176045), Sichuan Science and Technology Program (2025ZNSFSC0453 and 2024YFHZ0061), Sichuan Province Innovative Talent Funding Project for Postdoctoral Fellows, Sichuan Philosophy and Social Science Foundation Youth Program (SCJJ24ND217), Neuracle Cognitive EEG and tES Regulation Open Topics (BRKOT-UESTC-20231008L), and Sichuan Psychological Association Research Planning Program (SCSXLXH2023006).

Data availability

Data in this study were obtained from the ADNI database (<http://adni.loni.usc.edu>). Data used for validation is available from the OASIS dataset (<https://www.oasis-brains.org>). The datasets used and/or analyzed during the current study are available from the corresponding author upon reasonable request.

Declarations

Ethics approval and consent to participate

The ADNI study procedures were approved by the institutional review boards of all participating centers, and written informed consent was obtained from all participants or their authorized representatives according to the Declaration of Helsinki (consent for research). Ethics approval was obtained from the institutional review boards of each institution involved: Oregon Health and Science University; University of Southern California; University of California—San Diego; University of Michigan; Mayo Clinic, Rochester; Baylor College of Medicine; Columbia University Medical Center; Washington University, St. Louis; University of Alabama at Birmingham; Mount Sinai School of Medicine; Rush University Medical Center; Wien Center; Johns Hopkins University; New York University; Duke University Medical Center; University of Pennsylvania; University of Kentucky; University of Pittsburgh; University of Rochester Medical Center; University of California, Irvine; University of Texas Southwestern Medical School; Emory University; University of Kansas, Medical Center; University of California, Los Angeles; Mayo Clinic, Jacksonville; Indiana University; Yale University School of Medicine; McGill University, Montreal-Jewish General Hospital; Sunnybrook Health Sciences, Ontario; U.B.C. Clinic for AD & Related Disorders; Cognitive Neurology—St. Joseph's, Ontario; Cleveland Clinic Lou Ruvo Center for Brain Health; Northwestern University; Premiere Research Inst (Palm Beach Neurology); Georgetown University Medical Center; Brigham and Women's Hospital; Stanford University; Banner Sun Health Research Institute; Boston University; Howard University; Case Western Reserve University; University of California, Davis—Sacramento; Neurological Care of CNY; Parkwood Hospital; University of Wisconsin; University of California, Irvine—BIC; Banner Alzheimer's Institute; Dent Neurologic Institute; Ohio State University; Albany Medical College; Hartford Hospital, Olin Neuropsychiatry Research Center; Dartmouth-Hitchcock Medical Center; Wake Forest University Health Sciences; Rhode Island Hospital; Butler Hospital; UC San Francisco; Medical University South Carolina; St. Joseph's Health Care Nathan Kline Institute; University of Iowa College of Medicine; Cornell University and University of South Florida; USF Health Byrd Alzheimer's Institute. Investigators within the ADNI were involved in the design and implementation of ADNI and provided data, but did not participate in the analysis or writing of this report. A complete listing of ADNI investigators can be found at: http://adni.loni.usc.edu/wp-content/uploads/how_to_apply/ADNI_Acknowledgement_List.pdf. All participants in the OASIS-3 study were consented into Knight ADRC-related projects following procedures approved by the Institutional Review Board of Washington University School of Medicine. More details can be found online (<https://www.oasis-brains.org/>).

Competing interests

The authors declare no competing interests.

Received: 25 September 2024 / Accepted: 30 April 2025

Published online: 15 May 2025

References

- DeCarli C. Mild cognitive impairment: prevalence, prognosis, aetiology, and treatment. *Lancet Neurol.* 2003;2(1):15–21.
- Albert MS, Blacker D. Mild cognitive impairment and dementia. *Ann Rev Clin Psychol.* 2006;2:379–88.
- Nettiksimmmons J, DeCarli C, Landau S, Beckett L. Biological heterogeneity in ADNI amnesic mild cognitive impairment. *Alzheimer's Dement J Alzheimer's Assoc.* 2014;10(5):511–e521511.
- Wang X, Ye T, Zhou W, Zhang J. Uncovering heterogeneous cognitive trajectories in mild cognitive impairment: a data-driven approach. *Alzheimers Res Ther.* 2023;15(1):57.
- Petersen RC, Smith GE, Waring SC, Ivnik RJ, Tangalos EG, Kokmen E. Mild cognitive impairment: clinical characterization and outcome. *Arch Neurol.* 1999;56(3):303–8.
- Visser PJ, Kester A, Jolles J, Verhey F. Ten-year risk of dementia in subjects with mild cognitive impairment. *Neurology.* 2006;67(7):1201–7.
- Koepsell TD, Monsell SE. Reversion from mild cognitive impairment to normal or near-normal cognition: risk factors and prognosis. *Neurology.* 2012;79(15):1591–8.
- Dong A, Toledo JB, Honnorat N, Doshi J, Vargal E, Sotiras A, Wolk D, Trojanowski JQ, Davatzikos C. Heterogeneity of neuroanatomical patterns in prodromal Alzheimer's disease: links to cognition, progression and biomarkers. *Brain.* 2017;140(3):735–47.
- Young AL, Marinescu RV, Oxtoby NP, Bocchetta M, Yong K, Firth NC, Cash DM, Thomas DL, Dick KM, Cardoso J, et al. Uncovering the heterogeneity and Temporal complexity of neurodegenerative diseases with subtype and stage inference. *Nat Commun.* 2018;9(1):4273.
- Winblad B, Palmer K, Kivipelto M, Jelic V, Fratiglioni L, Wahlund LO, Nordberg A, Bäckman L, Albert M, Almkvist O, et al. Mild cognitive impairment—beyond controversies, towards a consensus: report of the international working group on mild cognitive impairment. *J Intern Med.* 2004;256(3):240–6.
- Tatsuoka C, Tseng H, Jaeger J, Varadi F, Smith MA, Yamada T, Smyth KA, Lerner AJ. Modeling the heterogeneity in risk of progression to Alzheimer's disease across cognitive profiles in mild cognitive impairment. *Alzheimers Res Ther.* 2013;5(2):14.
- Edmonds EC, Delano-Wood L, Clark LR, Jak AJ, Nation DA, McDonald CR, Libon DJ, Au R, Galasko D, Salmon DP, et al. Susceptibility of the conventional criteria for mild cognitive impairment to false-positive diagnostic errors. *Alzheimer's Dement J Alzheimer's Assoc.* 2015;11(4):415–24.
- Hughes TF, Snitz BE, Ganguli M. Should mild cognitive impairment be sub-typed? *Curr Opin Psychiatry.* 2011;24(3):237–42.
- Ezzati A, Zammit AR, Habeck C, Hall CB, Lipton RB. Detecting biological heterogeneity patterns in ADNI amnesic mild cognitive impairment based on volumetric MRI. *Brain Imaging Behav.* 2020;14(5):1792–804.
- Kikuchi M, Kobayashi K, Itoh S, Kasuga K, Miyashita A, Ikeuchi T, Yumoto E, Kosaka Y, Fushimi Y, Takeda T, et al. Identification of mild cognitive impairment subtypes predicting conversion to Alzheimer's disease using multimodal data. *Comput Struct Biotechnol J.* 2022;20:5296–308.
- Verdi S, Kia SM, Yong KXX, Tosun D, Schott JM, Marquand AF, Cole JH. Revealing individual neuroanatomical heterogeneity in Alzheimer disease using neuroanatomical normative modeling. *Neurology.* 2023;100(24):e2442–53.
- Avelar-Pereira B, Belloy ME, O'Hara R, Hosseini SMH. Decoding the heterogeneity of Alzheimer's disease diagnosis and progression using multilayer networks. *Mol Psychiatry.* 2023;28(6):2423–32.
- Tondelli M, Wilcock GK, Nichelli P, De Jager CA, Jenkinson M, Zamboni G. Structural MRI changes detectable up to ten years before clinical Alzheimer's disease. *Neurobiol Aging.* 2012;33(4):e825825–836.
- Bernard C, Helmer C, Dilharreguy B, Amieva H, Auriacombe S, Dartigues JF, Allard M, Catheline G. Time course of brain volume changes in the preclinical phase of Alzheimer's disease. *Alzheimer's Dement J Alzheimer's Assoc.* 2014;10(2):143–e151141.
- Kwak K, Giovanello KS, Bozoki A, Styner M, Dayan E. Subtyping of mild cognitive impairment using a deep learning model based on brain atrophy patterns. *Cell Rep Med.* 2021;2(12):100467.
- Zhao K, Zheng Q, Dyrba M, Rittman T, Li A, Che T, Chen P, Sun Y, Kang X, Li Q, et al. Regional radiomics similarity networks reveal distinct subtypes and abnormality patterns in mild cognitive impairment. *Advanced science (Weinheim, Baden-Wuerttemberg Germany).* 2022;9(12):e2104538.
- Baumeister H, Vogel JW, Insel PS, Kleineidam L, Wolfsgruber S, Stark M, Gellersen HM, Yakupov R, Schmid MC, Lüsebrink F et al. A generalizable data-driven model of atrophy heterogeneity and progression in memory clinic settings. *Brain.* 2024.
- Habes M, Grothe MJ, Tunc B, McMillan C, Wolk DA, Davatzikos C. Disentangling heterogeneity in Alzheimer's disease and related dementias using Data-Driven methods. *Biol Psychiatry.* 2020;88(1):70–82.
- Young AL, Oxtoby NP, Garbarino S, Fox NC, Barkhof F, Schott JM, Alexander DC. Data-driven modelling of neurodegenerative disease progression: thinking outside the black box. *Nat Rev Neurosci.* 2024;25(2):111–30.
- den Heijer T, van der Lijn F, Koudstaal PJ, Hofman A, van der Lugt A, Krestin GP, Niessen WJ, Breteler MM. A 10-year follow-up of hippocampal volume on magnetic resonance imaging in early dementia and cognitive decline. *Brain.* 2010;133(Pt 4):1163–72.
- Pegueroles J, Vilaplana E, Montal V, Sampedro F, Alcolea D, Carmona-Iragui M, Clarimon J, Blesa R, Lleó A, Fortea J. Longitudinal brain structural changes in preclinical Alzheimer's disease. *Alzheimer's Dement J Alzheimer's Assoc.* 2017;13(5):499–509.
- Dang M, Yang C, Chen K, Lu P, Li H, Zhang Z. Hippocampus-centred grey matter covariance networks predict the development and reversion of mild cognitive impairment. *Alzheimers Res Ther.* 2023;15(1):27.
- Mechelli A, Friston KJ, Frackowiak RS, Price CJ. Structural covariance in the human cortex. *J Neuroscience: Official J Soc Neurosci.* 2005;25(36):8303–10.
- Alexander-Bloch A, Giedd JN, Bullmore E. Imaging structural co-variance between human brain regions. *Nat Rev Neurosci.* 2013;14(5):322–36.
- Qing Z, Chen F, Lu J, Lv P, Li W, Liang X, Wang M, Wang Z, Zhang X, Zhang B. Causal structural covariance network revealing atrophy progression in Alzheimer's disease continuum. *Hum Brain Mapp.* 2021;42(12):3950–62.
- Montembeault M, Rouleau I, Provost JS, Brambati SM. Altered Gray Matter Structural Covariance Networks in Early Stages of Alzheimer's Disease. *Cerebral cortex (New York, NY: 1991).* 2016;26(6):2650–2662.
- Li K, Luo X, Zeng Q, Huang P, Shen Z, Xu X, Xu J, Wang C, Zhou J, Zhang M. Gray matter structural covariance networks changes along the Alzheimer's disease continuum. *NeuroImage Clin.* 2019;23:101828.
- Liu Z, Palaniyappan L, Wu X, Zhang K, Du J, Zhao Q, Xie C, Tang Y, Su W, Wei Y, et al. Resolving heterogeneity in schizophrenia through a novel systems approach to brain structure: individualized structural covariance network analysis. *Mol Psychiatry.* 2021;26(12):7719–31.
- LaMontagne PJ, Benzinger TLS, Morris JC, Keefe S, Hornbeck R, Xiong C, Grant E, Hassenstab J, Moulder K, Vlassenko AG et al. OASIS-3: longitudinal neuroimaging, clinical, and cognitive dataset for normal aging and Alzheimer disease. medRxiv. 2019 <https://doi.org/10.1101/2019.12.13.19014902>.
- Petersen RC, Aisen PS, Beckett LA, Donohue MC, Gamst AC, Harvey DJ, Jack CR Jr, Jagust WJ, Shaw LM, Toga AW, et al. Alzheimer's disease neuroimaging initiative (ADNI): clinical characterization. *Neurology.* 2010;74(3):201–9.
- O'Bryant SE, Waring SC, Cullum CM, Hall J, Lacritz L, Massman PJ, Lupo PJ, Reich JS, Doody R. Staging dementia using clinical dementia rating scale sum of boxes scores: a Texas Alzheimer's research consortium study. *Arch Neurol.* 2008;65(8):1091–5.
- Wei X, Du X, Xie Y, Suo X, He X, Ding H, Zhang Y, Ji Y, Chai C, Liang M et al. Mapping cerebral atrophic trajectory from amnesic mild cognitive impairment to Alzheimer's disease. *Cerebral cortex (New York, NY: 1991).* 2023;33(4):1310–1327.
- Zhang Y, Li X, Ji Y, Ding H, Suo X, He X, Xie Y, Liang M, Zhang S, Yu C, et al. MRAβ: A multimodal MRI-derived amyloid-β biomarker for Alzheimer's disease. *Hum Brain Mapp.* 2023;44(15):5139–52.
- Mohs RC, Knopman D, Petersen RC, Ferris SH, Ernesto C, Grundman M, Sano M, Bieliauskas L, Geldmacher D, Clark C, et al. Development of cognitive instruments for use in clinical trials of antedementia drugs: additions to the Alzheimer's disease assessment scale that broaden its scope. *The Alzheimer's disease cooperative study. Alzheimer Dis Assoc Disord.* 1997;11(Suppl 2):S13–21.

40. Folstein MF, Folstein SE, McHugh PR. Mini-mental State. A practical method for grading the cognitive State of patients for the clinician. *J Psychiatr Res*. 1975;12(3):189–98.
41. Estévez-González A, Kulisevsky J, Boltes A, Oterín P, García-Sánchez C. Rey verbal learning test is a useful tool for differential diagnosis in the preclinical phase of Alzheimer's disease: comparison with mild cognitive impairment and normal aging. *Int J Geriatr Psychiatry*. 2003;18(11):1021–8.
42. Tzourio-Mazoyer N, Landeau B, Papathanassiou D, Crivello F, Etard O, Delcroix N, Mazoyer B, Joliot M. Automated anatomical labeling of activations in SPM using a macroscopic anatomical parcellation of the MNI MRI single-subject brain. *NeuroImage*. 2002;15(1):273–89.
43. Fortin JP, Cullen N, Sheline YI, Taylor WD, Aselcioglu I, Cook PA, Adams P, Cooper C, Fava M, McGrath PJ, et al. Harmonization of cortical thickness measurements across scanners and sites. *NeuroImage*. 2018;167:104–20.
44. Guo X, Zhang X, Chen H, Zhai G, Cao Y, Zhang T, Gao L. Exploring the heterogeneity of brain structure in autism spectrum disorder based on individual structural covariance network. *Cerebral cortex (New York, NY: 1991)*. 2023;33(12):7311–7321.
45. Zheng C, Zhao W, Yang Z, Tang D, Feng M, Guo S. Resolving heterogeneity in Alzheimer's disease based on individualized structural covariance network. *Prog Neuro-psychopharmacol Biol Psychiatry*. 2024;129:110873.
46. Du X, Wei X, Ding H, Yu Y, Xie Y, Ji Y, Zhang Y, Chai C, Liang M, Li J, et al. Unraveling schizophrenia replicable functional connectivity disruption patterns across sites. *Hum Brain Mapp*. 2023;44(1):156–69.
47. Chai C, Ding H, Du X, Xie Y, Man W, Zhang Y, Ji Y, Liang M, Zhang B, Ning Y, et al. Dissociation between neuroanatomical and symptomatic subtypes in schizophrenia. *Eur Psychiatry: J Association Eur Psychiatrists*. 2023;66(1):e78.
48. Ewers M, Franzmeier N, Suárez-Calvet M, Morenas-Rodríguez E, Caballero MAA, Kleinberger G, Piccio L, Cruchaga C, Deming Y, Dichgans M et al. Increased soluble TREM2 in cerebrospinal fluid is associated with reduced cognitive and clinical decline in Alzheimer's disease. *Science translational medicine*. 2019;11(507).
49. Bernal-Rusiel JL, Greve DN, Reuter M, Fischl B, Sabuncu MR. Statistical analysis of longitudinal neuroimage data with linear mixed effects models. *NeuroImage*. 2013;66:249–60.
50. Hsiung GY, Sadovnick AD, Feldman H. Apolipoprotein E epsilon4 genotype as a risk factor for cognitive decline and dementia: data from the Canadian study of health and aging. *CMAJ: Can Med Association J = J De l'Association Medicale Canadienne*. 2004;171(8):863–7.
51. Arnatkeviciute A, Fulcher BD, Fornito A. A practical guide to linking brain-wide gene expression and neuroimaging data. *NeuroImage*. 2019;189:353–67.
52. Abdi H. Partial least squares regression and projection on latent structure regression (PLS Regression). *Wiley Interdisciplinary Reviews: Comput Stat*. 2010;2:97–106.
53. Váša F, Seidlitz J, Romero-García R, Whitaker KJ, Rosenthal G, Vértes PE, Shinn M, Alexander-Bloch A, Fonagy P, Dolan RJ et al. Adolescent Tuning of Association Cortex in Human Structural Brain Networks. *Cerebral cortex (New York, NY: 1991)*. 2018;28(1):281–294.
54. Whitaker KJ, Vértes PE, Romero-García R, Váša F, Moutoussis M, Prabhu G, Weiskopf N, Callaghan MF, Wagstyl K, Rittman T, et al. Adolescence is associated with genomically patterned consolidation of the hubs of the human brain connectome. *Proc Natl Acad Sci USA*. 2016;113(32):9105–10.
55. Morgan SE, Seidlitz J, Whitaker KJ, Romero-García R, Clifton NE, Scarpazza C, van Amelsvoort T, Marcelis M, van Os J, Donohoe G, et al. Cortical patterning of abnormal morphometric similarity in psychosis is associated with brain expression of schizophrenia-related genes. *Proc Natl Acad Sci USA*. 2019;116(19):9604–9.
56. Zhou Y, Zhou B, Pache L, Chang M, Khodabakhshi AH, Tanaseichuk O, Benner C, Chanda SK. Metascape provides a biologist-oriented resource for the analysis of systems-level datasets. *Nat Commun*. 2019;10(1):1523.
57. Liu Z, Rolls ET, Liu Z, Zhang K, Yang M, Du J, Gong W, Cheng W, Dai F, Wang H, et al. Brain annotation toolbox: exploring the functional and genetic associations of neuroimaging results. *Bioinf (Oxford England)*. 2019;35(19):3771–8.
58. Rolls ET, Joliot M, Tzourio-Mazoyer N. Implementation of a new parcellation of the orbitofrontal cortex in the automated anatomical labeling atlas. *NeuroImage*. 2015;122:1–5.
59. Rolls ET, Huang CC, Lin CP, Feng J, Joliot M. Automated anatomical labelling atlas 3. *NeuroImage*. 2020;206:116189.
60. Fan L, Li H, Zhuo J, Zhang Y, Wang J, Chen L, Yang Z, Chu C, Xie S, Laird AR et al. The Human Brainnetome Atlas: A New Brain Atlas Based on Connectional Architecture. *Cerebral cortex (New York, NY: 1991)*. 2016;26(8):3508–3526.
61. Hubert L, Arabie P. Comparing partitions. *J Classif*. 1985;2(1):193–218.
62. Bassett DS, Sporns O. Network neuroscience. *Nat Neurosci*. 2017;20(3):353–64.
63. Evans AC. Networks of anatomical covariance. *NeuroImage*. 2013;80:489–504.
64. Lin SY, Lin CP, Hsieh TJ, Lin CF, Chen SH, Chao YP, Chen YS, Hsu CC, Kuo LW. Multiparametric graph theoretical analysis reveals altered structural and functional network topology in Alzheimer's disease. *NeuroImage Clin*. 2019;22:101680.
65. Han S, Zheng R, Li S, Zhou B, Jiang Y, Fang K, Wei Y, Pang J, Li H, Zhang Y, et al. Resolving heterogeneity in depression using individualized structural covariance network analysis. *Psychol Med*. 2023;53(11):5312–21.
66. Chételat G, Landeau B, Eustache F, Mézenge F, Viader F, de la Sayette V, Desgranges B, Baron JC. Using voxel-based morphometry to map the structural changes associated with rapid conversion in MCI: a longitudinal MRI study. *NeuroImage*. 2005;27(4):934–46.
67. Dai Z, He Y. Disrupted structural and functional brain connectomes in mild cognitive impairment and Alzheimer's disease. *Neurosci Bull*. 2014;30(2):217–32.
68. Billelo M, Doshi J, Nabavizadeh SA, Toledo JB, Erus G, Xie SX, Trojanowski JQ, Han X, Davatzikos C. Correlating cognitive decline with white matter lesion and brain atrophy magnetic resonance imaging measurements in Alzheimer's disease. *J Alzheimer's Disease: JAD*. 2015;48(4):987–94.
69. Edmonds EC, Thomas KR, Rapsak SZ, Lindemer SL, Delano-Wood L, Salmon DP, Bondi MW. Data-driven classification of cognitively normal and mild cognitive impairment subtypes predicts progression in the NACC dataset. *Alzheimer's Dement J Alzheimer's Assoc*. 2024;20(5):3442–54.
70. Nezhadmoghadam F, Martínez-Torteya A, Treviño V, Martínez E, Santos A, Tamez-Peña J. Alzheimer's disease neuroimaging I: robust discovery of mild cognitive impairment subtypes and their risk of Alzheimer's disease conversion using unsupervised machine learning and Gaussian mixture modeling. *Curr Alzheimer Res*. 2021;18(7):595–606.
71. Katabathula S, Davis PB, Xu R. Comorbidity-driven multi-modal subtype analysis in mild cognitive impairment of Alzheimer's disease. *Alzheimer's Dement J Alzheimer's Assoc*. 2023;19(4):1428–39.
72. Edmonds EC, Eppig J, Bondi MW, Leyden KM, Goodwin B, Delano-Wood L, McDonald CR. Heterogeneous cortical atrophy patterns in MCI not captured by conventional diagnostic criteria. *Neurology*. 2016;87(20):2108–16.
73. Mattsson N, Zetterberg H, Hansson O, Andreassen N, Parnetti L, Jonsson M, Herukka SK, van der Flier WM, Blankenstein MA, Ewers M, et al. CSF biomarkers and incipient alzheimer disease in patients with mild cognitive impairment. *JAMA*. 2009;302(4):385–93.
74. Dark HE, An Y, Duggan MR, Joyner C, Davatzikos C, Erus G, Lewis A, Moghekar AR, Resnick SM, Walker KA. Alzheimer's and neurodegenerative disease biomarkers in blood predict brain atrophy and cognitive decline. *Alzheimers Res Ther*. 2024;16(1):94.
75. Jansen IE, Savage JE, Watanabe K, Bryois J, Williams DM, Steinberg S, Sealock J, Karlsson IK, Hägg S, Athanasiu L, et al. Genome-wide meta-analysis identifies new loci and functional pathways influencing Alzheimer's disease risk. *Nat Genet*. 2019;51(3):404–13.
76. Susanto TA, Pua EP, Zhou J. Cognition, brain atrophy, and cerebrospinal fluid biomarkers changes from preclinical to dementia stage of Alzheimer's disease and the influence of Apolipoprotein e. *J Alzheimer's Disease: JAD*. 2015;45(1):253–68.
77. Emrani S, Arain HA, DeMarshall C, Nuriel T. APOE4 is associated with cognitive and pathological heterogeneity in patients with Alzheimer's disease: a systematic review. *Alzheimers Res Ther*. 2020;12(1):141.
78. Wang L, Yin YL, Liu XZ, Shen P, Zheng YG, Lan XR, Lu CB, Wang JZ. Current Understanding of metal ions in the pathogenesis of Alzheimer's disease. *Translational Neurodegeneration*. 2020;9:10.
79. Tzioras M, McGeachan RI, Durrant CS, Spire-Jones TL. Synaptic degeneration in alzheimer disease. *Nat Reviews Neurol*. 2023;19(1):19–38.
80. Mufson EJ, Binder L, Counts SE, DeKosky ST, de Toledo-Morrell L, Ginsberg SD, Ikonomic MD, Perez SE, Scheff SW. Mild cognitive impairment: pathology and mechanisms. *Acta Neuropathol*. 2012;123(1):13–30.
81. Harper L, Barkhof F, Fox NC, Schott JM. Using visual rating to diagnose dementia: a critical evaluation of MRI atrophy scales. *J Neurol Neurosurg Psychiatry*. 2015;86(11):1225–33.

82. Frizzell TO, Glashutter M, Liu CC, Zeng A, Pan D, Hajra SG, D'Arcy RCN, Song X. Artificial intelligence in brain MRI analysis of Alzheimer's disease over the past 12 years: A systematic review. *Ageing Res Rev.* 2022;77:101614.
83. Zhang H, Wang Z, Wang J, Lyu X, Wang X, Liu Y, Zeng X, Yuan H, Wang H, Yu X. Computerized multi-domain cognitive training reduces brain atrophy in patients with amnesic mild cognitive impairment. *Translational Psychiatry.* 2019;9(1):48.
84. Diaz-Galvan P, Lorenzon G, Mohanty R, Mårtensson G, Cavedo E, Lista S, Vergallo A, Kantarci K, Hampel H, Dubois B, et al. Differential response to

donepezil in MRI subtypes of mild cognitive impairment. *Alzheimers Res Ther.* 2023;15(1):117.

Publisher's note

Springer Nature remains neutral with regard to jurisdictional claims in published maps and institutional affiliations.